

Investigation of the effect of water content on the mechanical behavior of track-bed materials under various coarse grain contents

Yu Su, Yu-Jun Cui, Jean-Claude Dupla, Jean Canou

▶ **To cite this version:**

Yu Su, Yu-Jun Cui, Jean-Claude Dupla, Jean Canou. Investigation of the effect of water content on the mechanical behavior of track-bed materials under various coarse grain contents. Construction and Building Materials, 2020, 263, pp.120206. 10.1016/j.conbuildmat.2020.120206 . hal-03045809

HAL Id: hal-03045809
https://enpc.hal.science/hal-03045809

Submitted on 22 Aug 2022

HAL is a multi-disciplinary open access archive for the deposit and dissemination of scientific research documents, whether they are published or not. The documents may come from teaching and research institutions in France or abroad, or from public or private research centers.

L'archive ouverte pluridisciplinaire **HAL**, est destinée au dépôt et à la diffusion de documents scientifiques de niveau recherche, publiés ou non, émanant des établissements d'enseignement et de recherche français ou étrangers, des laboratoires publics ou privés.



Distributed under a Creative Commons Attribution - NonCommercial 4.0 International License

Version of Record: https://www.sciencedirect.com/science/article/pii/S095006182032211X
Manuscript_a8210f0772d588285e4f4f466769622c

Investigation of the effect of water content on the mechanical behavior of track-bed materials under various coarse grain contents

Yu Su, Yu-Jun Cui, Jean-Claude Dupla, Jean Canou

Laboratoire Navier/CERMES, Ecole des Ponts ParisTech (ENPC), France

Corresponding author

Professor Yu-Jun Cui

Ecole des Ponts ParisTech, Laboratoire Navier/CERMES, 6 – 8 av. Blaise Pascal, Cité Descartes, Champs-sur-Marne, 77455 Marne – la – Vallée cedex 2, France

Tel.: +33 164153550

Fax: +33 164153562

E-mail address: yu-jun.cui@enpc.fr

© 2020 published by Elsevier. This manuscript is made available under the CC BY NC user license
https://creativecommons.org/licenses/by-nc/4.0/

Abstract

In the French conventional railway track, an interlayer was created naturally through the interpenetration of ballast and subgrade under the effect of long-term train loading. Field investigation showed that the proportion of ballast grains decreased over depth in the interlayer. Moreover, the water content of interlayer soils varies depending on the weather conditions, which can strongly affect the mechanical behavior of interlayer soil. In this study, the effect of water content on the mechanical behavior of interlayer soils under various coarse grain contents was investigated by monotonic triaxial tests. Three water contents (w = 17.6%, 10.6%, and 7.0%), five volumetric coarse grain contents (f_v = 0%, 10%, 20%, 35%, and 45%) and three confining pressures (σ_3 = 30 kPa, 60 kPa and 120 kPa) were considered. Results showed that a decrease of w led to an increase of shear strength and soil stiffness due to the effect of suction, and to an increase of dilatancy due to the aggregation of fine soils. Moreover, the variations of maximum deviator stress q_{max}, Young's modulus E_0, dilatancy angle ψ and friction angle φ with f_v followed a bi-linear pattern for the three σ_3 values, defining a characteristic volumetric coarse grain content $f_{v\text{-}cha}$ value for a given w value: $f_{v\text{-}cha} \approx$ 25%, 29% and 33% for w = 17.6%, 10.6% and 7.0%, respectively. The $f_{v\text{-}cha}$ corresponded to the transition from a structure dominated by fine soils to a structure dominated by coarse grains. The increase of $f_{v\text{-}cha}$ with the decrease of w could be attributed to the swelling and shrinkage of fines. While drying from optimum water content of fines $w_{opt\text{-}f}$ =13.7% to a lower w_f value, more coarse grains were needed to constitute the global skeleton due to the increase of the global volume of macro-pores resulted from the shrinkage of fine soils. By contrast, while wetting from $w_{opt\text{-}f}$ =13.7% to a higher w_f value, since the global volume of macro-pores

43 decreased due to the swelling of fine soils, less coarse grains were required to constitute the
44 global skeleton.

45 **Keywords:** fabric/structure of soils; partial saturation; laboratory tests; compaction; shear
46 strength

INTRODUCTION

Most French conventional railway track was constructed by putting the ballast layer on the subgrade soil directly. Due to the long-term train circulation, a layer namely interlayer was naturally formed in the substructure, mainly by the interpenetration of ballast and subgrade. Considering its high dry density (2.4 Mg /m^3) and high bearing capacity [1], the French railway company (SNCF) has decided to keep it as part of the substructure in the execution of the track renewal program [2].

Based on the field investigation, the content of ballast grains was found to decrease over depth [1]. Globally, the interlayer can be separated into two parts: the upper part dominated by ballast grains and the lower part dominated by fine soils. For the upper part, the effects of fine soils content and water content on the mechanical behavior were studied by Trinh et al. [3], Cui et al. [2], Duong et al. [4-6] and Lamas-Lopez et al. [7, 8] by performing monotonic and cyclic triaxial tests. In order to extend the study to the whole interlayer, Wang et al. [9-11] and Qi et al. [12] investigated the effect of coarse grain content f_v (volumetric ratio of coarse grains to total sample) on the mechanical behavior. Results revealed existence of a characteristic volumetric coarse grain content $f_{v\text{-}cha}$, below which the soil was characterised by a fine matrix with coarse grains floating in it, while beyond which the soil was characterised by a coarse grain skeleton. It is worth noting that in the previous studies, the effect of f_v on the mechanical behavior was investigated under constant water content conditions. This is obviously not the field condition where the water content varies depending on the weather conditions, resulting in changes in mechanical behavior. Therefore, from a practical point of

68 view, it appears essential to investigate the effect of water content on the mechanical behavior
69 of interlayer soil.

70 There are several studies addressing the effect of coarse grain content on the mechanical
71 behavior of soil. Seif El Dine et al. [13] worked on sandy matrix with f_v of gravels, showing
72 an increase of shear strength with the increase of f_v. However, Vallejo [14] showed an
73 opposite trend when the mass proportion of coarse particles was beyond 65% for a mixture of
74 rock and sand. It is worth noting that the fines involved in their studies were cohesionless soils
75 like sand and glass beads, which did not represent the natural fine soils in the interlayer. Wang
76 et al. [9-11] studied the effect of f_v on the static and dynamic responses of interlayer soil, and
77 identified a characteristic value $f_{v\text{-}cha}$ that could be used to differentiate two distinct soil fabrics.
78 Qi et al. [12] investigated the effect of the coefficient of uniformity C_u of coarse grains on the
79 mechanical behavior of interlayer soils, and found that the decrease of C_u led to an increase of
80 $f_{v\text{-}cha}$. A few studies were undertaken to investigate the water content effect on the mechanical
81 behavior of substructure soils in terms of shear strength, resilient modulus, etc. Trinh et al. [3]
82 investigated the effect of water content on the mechanical behavior of fouled ballast at
83 different water contents and found that the lower the water content, the higher the shear
84 strength. Duong et al. [6] studied the effect of water content on the resilient modulus of the
85 upper part interlayer soil by large-scale cyclic triaxial tests, and reported that the increase of
86 water content gave rise to a decrease of resilient modulus. To the author's knowledge, there
87 has been no work addressing the effect of water content on $f_{v\text{-}cha}$.

88 In this study, the effect of water content on the mechanical behavior of the interlayer soil
89 at various f_v values was investigated by performing monotonic triaxial tests under different

confining pressures. Three water contents (17.6%, 10.6%, and 7.0%), five coarse grain contents (0%, 10%, 20%, 35%, and 45%) and three confining pressures (30 kPa, 60 kPa and 120 kPa) were considered. The mechanical properties including Young's modulus E_0, Poisson's ratio v, dilatancy angle ψ, friction angle φ and cohesion c were analyzed. The results obtained allowed the effect of water content on the characteristic volumetric coarse grain content $f_{v\text{-}cha}$ to be clarified.

MATERIALS AND METHODS

Materials and sample preparation

Since it was difficult to obtain intact interlayer soil, the studied soil was reconstituted in the laboratory. For the fines, in order to simulate the grain size distribution of fine soils from 'Senissiat site' (Fig. 1), nine different commercial soils including sand and clay were mixed, with the pre-determined proportions shown in Table 1. The liquid limit and plasticity index of the reconstituted fine soil were 32% and 20%, respectively defining the fine soil as CL according to the universal soil classification system (Fig. 2). A good agreement between real fine soil and reconstituted fine soil was observed in terms of grain size distribution (Fig. 1), liquid limit and plasticity index (Fig. 2). Standard Proctor compaction was performed following ASTM D698-12 [15] for the reconstituted fine soil (Fig. 3), allowing an optimum water content $w_{opt\text{-}f}$ = 13.7% and a maximum dry density $\rho_{dmax\text{-}f}$ = 1.82 Mg/m^3 to be identified.

For the coarse grains, following the parallel similitude method adopted by Wang et al. [10] and Qi et al. [12], micro-ballast was prepared to represent the real ballast by using three granular materials G 4-10, HN 2-4 and G 10-20, as shown in Fig. 4. In order to quantify the

amount of micro-ballast in a sample, a parameter namely volumetric coarse grain content f_v [9-13] was adopted:

$$f_v = V_{in} / V_{total} \quad (1)$$

where V_{in} and V_{total} represent the coarse grain volume and the total sample volume, respectively. Note that the total sample volume V_{total} was composed of the coarse grain volume V_{in} and the fine soil volume V_{fines}. The dry density of fine soil in all samples was controlled at $\rho_{dmax\text{-}f}$ = 1.82 Mg/m^3 (Table 2). At a given f_v value, the dry mass of coarse grain, the dry mass of fine soil and the water content contained in the fine soil can be calculated. Details about the calculation could be found in Wang et al. [10].

For the preparation of samples at target f_v and w_f, the fine soil was prepared at optimum water content $w_{opt\text{-}f}$ = 13.7%, then stored in a container for 24 h for moisture homogenization. The fine soil was then mixed with micro-ballast grains thoroughly to reach the target f_v value. After that, the soil mixture was dynamically compacted in three layers to reach the size of 100 mm diameter and 200 mm height. Note that at a given compaction effort, the dry density of fine soils changes with the variation of coarse grain content f_v. Since the dry density of fine soil in all samples was controlled at $\rho_{dmax\text{-}f}$ = 1.82 Mg/m^3, the compaction efforts was higher for the samples at higher f_v values. As a result, higher ρ_d values were obtained for the samples with higher f_v values, as shown in Table 2.

After reaching the target f_v value, either a wetting or a drying process was adopted to obtain the target w_f: w_1 = 17.6% on the wet side of optimum; w_2 = 10.6% and w_3 = 7.0% on the dry side of optimum. In the case of drying process, considering that a too fast drying would

lead to sample damage by fissuring, a milder drying method was performed: the sample was exposed to the air in the laboratory for 1 h each time, and then enveloped with plastic film for equilibration. The time of equilibration needed was determined by measurement of suction and water content in three positions: in the center, ½ r and r, with r being radius of the sample. The results obtained showed that 7 h was required for reaching reasonable equilibration in terms of suction and water content (Table 3). In the case of wetting process, 10 g water was sprayed on the sample each time prior to covering it with plastic film for equilibration. The same equilibration time of at least 7 h was adopted.

When wetting or drying to a target w_f, the volume of sample was measured by means of a caliper. The volume changes from initial water content $w_{opt\text{-}f}$ = 13.7% to different target w_f values are presented in Fig. 5. It appears that at a given f_v value, an increase of water content from $w_{opt\text{-}f}$ = 13.7% to w_1= 17.6% led to sample swelling, while a decrease of water content from $w_{opt\text{-}f}$ = 13.7% to w_2= 10.6% or w_3= 7.0% led to sample shrinkage. Moreover, under a given water content, the sample exhibited lower swelling-shrinkage with higher f_v values, illustrating the sensitivity of fine soil to water content changes. The measured dry densities of samples after wetting or drying are shown in Table 2.

Monotonic triaxial tests

The mechanical behavior of soil at five different f_v values (0%, 10%, 20%, 35%, and 45%) and three different w_f contents (17.6%, 10.6%, and 7.0%) was investigated by monotonic triaxial tests, under three different σ_3 values (30 kPa, 60 kPa and 120 kPa). Note that all

154 samples were prepared to reach the target water contents (w_1 = 17.6% on the wet side, or w_2 =
155 10.6% and w_3 = 7.0% on the dry side) prior to starting the test. For the samples at w_1 = 17.6%
156 (S_r = 100%), an overnight consolidation under the corresponding confining pressure was
157 adopted prior to shearing, to ensure the dissipation of pore water pressure. On the contrary, for
158 the samples at w_2 = 10.6% (S_r = 60%) or w_3 = 7.0% (S_r = 40%), after an application of σ_3, the
159 sample was directly sheared, because only air was expected to be expelled. A shear rate as
160 low as 0.1mm/min was adopted for all tests. The tests ended when a peak deviator stress
161 appeared or the axial strain ε_1 reached 15% in case without occurrence of peak deviator stress.

162

163 EXPERIMENTAL RESULTS

164 *Variation of shear behavior with f_v*

165 The variations of deviator stress q and volumetric strain ε_v with axial strain ε_1 for samples at
166 w_1 = 17.6% and five different f_v values are depicted in Fig. 6. It can be observed from Figs.
167 6a$_1$-6a$_3$ that under a given confining pressure σ_3 value, the maximum deviator stress q_{max}
168 increased slowly with the increase of f_v for $f_v \leq 20\%$, while the increase of q_{max} was more
169 pronounced for $f_v \geq 35\%$. The similar phenomena can be observed for the case of w_2 = 10.6%
170 and w_3 = 7.0%.

171 In Fig. 6b$_1$, pure contractancy behaviour was observed for samples at $f_v \leq 20\%$, while for
172 samples at $f_v \geq 35\%$, a behavior of contractancy followed by dilatancy was identified.
173 Moreover, the larger the f_v value, the more pronounced the dilatancy behaviour. This dilatancy

174 was however reduced by the increase of confining pressure: when σ_3 was increased from 60
175 kPa (Fig. 6b$_2$) to 120 kPa (Fig. 6b$_3$), the contractancy increased and the dilatancy decreased.

176

177 *Variation of maximum deviator stress q_{max} with w*

178 Fig. 7 depicts the variations of q_{max} against f_v at different σ_3 values for three different water
179 contents. In the case of w_1 = 17.6% (Fig. 7a), it appeared that under a given σ_3 value, the
180 variation of q_{max} followed a bi-linear pattern with two different slopes, which defined a
181 characteristic volumetric coarse grain content $f_{v\text{-}cha}$. Moreover, similar $f_{v\text{-}cha}$ values (around
182 25%) could be identified for the three different σ_3 values. Physically, the $f_{v\text{-}cha}$ value
183 distinguished two different soil fabrics: when $f_v \leq f_{v\text{-}cha}$, the soil fabric was governed by fine
184 soil dominated structure, while when $f_v \geq f_{v\text{-}cha}$ it was governed by coarse grain dominated
185 structure, in agreement with the observations by Wang et al. [10] and Qi et al. [12].

186 The same phenomena were observed for the two other water contents: w_2 = 10.6% (Fig.
187 7b) and w_3 = 7.0% (Fig. 7c). For each water content, q_{max} varies in a bi-linear fashion with
188 with f_v, defining a $f_{v\text{-}cha}$ value which is independent of the σ_3 value. The values of $f_{v\text{-}cha}$ were 29%
189 and 33% for w_2 = 10.6% and w_3 = 7.0%, respectively. Comparison of the $f_{v\text{-}cha}$ values at
190 different water contents showed that $f_{v\text{-}cha}$ increased with the decrease of water content.

191

192 *Variation of Young's modulus E_0 with w*

In this study, the Young's modulus E_0, was defined as the ratio of deviator stress to axial strain from 0% to 1%. Fig. 8 shows the variations of E_0 with f_v under different σ_3 values for the three water contents. The effect of w on Young's modulus E_0 can be clearly observed: at a given f_v and σ_3, E_0 increased with the decrease of water content. This was attributed to the increase of suction with the decrease of water content. At a given water content, a bi-linear fitting could be also applied to represent changes of E_0 with f_v for all σ_3 values. This also defined a characteristic volumetric coarse grain content $f_{v\text{-}cha}$, which was independent of σ_3. As far as the variation of $f_{v\text{-}cha}$ with w was concerned, it appeared from Fig. 8 that $f_{v\text{-}cha}$ increased with the decrease of w: $f_{v\text{-}cha}$ was around 25% for w_1 = 17.6% (Fig. 8a), 29% for w_2 = 10.6% (Fig. 8b) and 33% for w_3 = 7% (Fig. 8c), which agreed well with the previous observation while studying the effect of water content on q_{max} in Fig. 7.

Variations of Poisson's ratio v and dilatancy angle ψ with w

Based on the volumetric strain-axial strain curves, the Poisson's ratio v and the dilatancy angle ψ were determined using respectively Eqs. (1) and (2) [16]:

$$v = (1- k_c)/2 \quad (1)$$

$$\sin \psi = k_D/(-2+ k_D) \quad (2)$$

where k_c and k_D are the slopes of volumetric strain-axial strain curves in the contractancy phase and dilatancy phase, respectively.

Fig. 9 depicts the variations of Poisson's ratio v versus f_v at different σ_3 values for three water contents. At $w_1 = 17.6\%$ (Fig. 9a), v was not significantly influenced by σ_3 and f_v, with the values fluctuating around $v = 0.36$. The values of v at $f_v \leq 20\%$ were slightly larger than those at $f_v \geq 35\%$. This was due to the transition of soil fabric from fine soils dominated structure to coarse grains dominated structure, which resulted in the increase of soil stiffness and the decrease of horizontal strain. Moreover, the difference of v between $f_v \leq 20\%$ and $f_v \geq 35\%$ decreased with the decrease of water content. The average value of v was 0.21 at $w_2 = 10.6\%$ (Fig. 9b) and 0.19 at $w_3 = 7.0\%$ (Fig. 9c). At $w_3 = 7.0\%$, the v remained almost unchanged with the increase of f_v. Overall, it appeared that the average value of v decreased with the decreasing water content, suggesting that the lateral strain was reduced by the increase of suction or decrease of water content.

The effect of w on the dilatancy angle ψ can be clearly observed in Fig. 10: under given f_v and σ_3 values, the ψ increased with the decrease of w. This could be attributed to the aggregation of fine soil induced by the increase of suction. Indeed, a lower water content would generate a higher suction. In that case, the fine soils behaved more like granular materials, exhibiting more dilatancy behavior, as shown by Cui and Delage [17] and Ng et al. [18].

As shown in Fig. 10a ($w_1 = 17.6\%$), no dilatancy behavior was observed for f_v varying from 0% to 20% at all σ_3 values, whereas an obvious dilatancy behaviour was observed for $f_v = 35\%$ at $\sigma_3 = 30$ kPa and for $f_v = 45\%$ at all σ_3 values. In addition, in Fig. 10b and Fig. 10c, a distinct change of ψ was observed from $f_v \leq 20\%$ to $f_v \geq 35\%$, defining a value of characteristic

233 volumetric coarse grain content $f_{v\text{-}cha} \approx 29\%$ at $w_2 = 10.6\%$ and $f_{v\text{-}cha} \approx 33\%$ at $w_3 = 7.0\%$. This
234 increase of $f_{v\text{-}cha}$ with the decrease of water content was consistent with the observation of
235 water effect on q_{max} and E_0.

236

237 *Variations of cohesion c and friction angle φ with w*

238 The values of cohesion c and friction angle φ were determined based on the peak deviator
239 stress values. Fig.11 depicts the variation of cohesion c with w. It can be observed that at a
240 given f_v, the cohesion c increased with the decrease of water content. This could be attributed
241 to the effect of suction on the fine soil.

242 For the friction angle φ, Fig.12 shows that φ increased with the decrease of w. This
243 confirmed the aggregation phenomenon with the decrease of w for the fine soils. The similar
244 observation was made by Zhao et al. [19] while studying the shear strength of a mixture of
245 sand, silt and gravel. Moreover, under a given w, a bi-linear pattern of increasing trend with f_v
246 was observed for φ. A value of $f_{v\text{-}cha}$ could be thus identified for each water content: $f_{v\text{-}cha} \approx$
247 25%, 29%, 33% for $w = 17.6\%$, 10.6%, 7.0%, respectively, in agreement with the effects of
248 water content on q_{max}, E_0 and ψ.

249

250 DISCUSSIONS

251 The test results showed that the value of $f_{v\text{-}cha}$ increased with the decrease of water content, as
252 shown in Table 4. Wang et al. [10] obtained a value of $f_{v\text{-}cha}$ equal to 27% at the optimum

253 water content $w_{opt\text{-}f}$ = 13.7%, which came to confirm the observation made in this study.

254 As mentioned before, the $f_{v\text{-}cha}$ corresponded to the transition of soil fabric: when $f_v \leq f_{v\text{-}cha}$,
255 the soil fabric was the fine soils dominated structure, while when $f_v \geq f_{v\text{-}cha}$, the soil fabric
256 changed to the coarse grains dominated structure. In other words, the $f_{v\text{-}cha}$ represented the
257 minimum f_v value needed for forming a coarse grains dominated structure. When $f_v \geq f_{v\text{-}cha}$,
258 two categories of fine soils were expected, namely a first category of dense fine soils situated
259 between coarse grains and a second category of loose fine soils situated in the macro-pores
260 surrounded by coarse grains. The former contributed to the loading-bearing skeleton of coarse
261 grains, whereas the latter contributed little, as concluded by de Frias Lopez [20] through
262 discrete element analysis.

263 The variation of $f_{v\text{-}cha}$ with w could be attributed to the swelling upon wetting and
264 shrinkage upon drying of these two categories of fines. With the decrease of water content, the
265 two categories of fine soils would shrink. The shrinkage of the first category of fines would
266 lead to a decrease of macro-pores between coarse grains, while the shrinkage of the second
267 category would lead to an increase of macro-pores surrounded by coarse grains. As the
268 density was expected to be higher and the quantity was expected to be smaller for the first
269 category of fines, the decrease of macro-pores volume due to the shrinkage of the first
270 category of fines was expected to be much smaller than the increase of macro-pores volume
271 due to the shrinkage of the second category of fines. This was supported by the observation
272 from Zhang and Li [21] using mercury intrusion porosimetry, who studied the fine/coarse soil
273 mixture and reported that the structure supported by coarse grains was stable, and thus the
274 shrinkage of clayey soils gave rise to an increase of the volume of macro-pores surrounded by

coarse particles. The effect of shrinkage of fine soils was also observed by Fies et al. [22] for the ternary mixtures of sand, silt and clay soils. They reported that when the fine fraction contained larger than 25% clay content, the shrinkage of fine fraction gave rise to the formation of macro-pores among the coarse fraction. It is worth noting that in this study, 30% of clay content of Speswhite and Bentonite were shown in Table 1 for the fine fraction, which contributed to the formation of macro-pores in the coarse grain skeleton. Thus, with the increase of volume of macro-pores, more coarse grains were needed to constitute a global skeleton. This is characterized by the increase of $f_{\text{v-cha}}$ value.

CONCLUSIONS

The effect of w on the mechanical behavior of interlayer soil at various f_{v} was investigated by monotonic triaxial tests. Three water contents (w = 17.6%, 10.6%, and 7.0%), five volumetric coarse grain contents (f_v = 0%, 10%, 20%, 35% and 45%) and three confining pressures (σ_3 = 30 kPa, 60 kPa and 120 kPa) were considered. The obtained results allowed the following conclusions to be drawn.

The decrease of water content led to an increase of the peak deviator stress q_{max} and the Young's modulus E_0. This could be explained by the effect of suction with the decrease of water content. The Poisson's ratio v was found to decrease with the decrease of water content, because the horizontal deformation was reduced by the increase of suction. The dilatancy angle ψ and the friction angle φ were found to increase with the decrease of water content. This was attributed to the aggregation of fine soils induced by the increase of suction,

296 enhancing the dilatancy behavior and the friction of soil. A larger cohesion c was observed at
297 lower w, also due to the effect of suction in fine soils.

298 The variation of q_{max}, E_0, ψ, and φ with f_v followed a bi-linear pattern, defining a same
299 characteristic $f_{v\text{-}cha}$ value for a given w value: $f_{v\text{-}cha} \approx 25\%$, 29% and 33% for w = 17.6%, 10.6%
300 and 7.0%, respectively. The value of $f_{v\text{-}cha} \approx 27\%$ at w_{opt} = 13.7% reported by Wang et al.
301 (2018a) came to support this observation. This was attributed to the swelling upon wetting and
302 shrinkage upon drying of two categories of fine soils: a first category of dense fine soil
303 situated between coarse grains and a second category of loose fine soil situated in the macro-
304 pores surrounded by coarse grains. With the decrease of water content, the two categories of
305 fine soils would shrink. Moreover, the shrinkage of the first category of fines would lead to a
306 decrease of macro-pores between coarse grains, while the shrinkage of the second category
307 would lead to an increase of macro-pores surrounded by coarse grains. As the decrease of
308 macro-pores volume due to the shrinkage of the first category of fines was expected to be
309 much smaller than the increase of macro-pores volume due to the shrinkage of the second
310 category of fines, the global macro-pores volume was increasing with the decrease of water
311 content. In that case, more coarse grains were needed to constitute a global skeleton, leading
312 to an increase of $f_{v\text{-}cha}$.

313

314 ACKNOWLEDGEMENTS

315 This work was supported by the Chinese Scholar Council (CSC) and Ecole des Ponts
316 ParisTech.

317

318 REFERENCES

319 [1] V. N. Trinh, Comportement hydromécanique des matériaux constitutifs de plateformes
320 ferroviaires anciennes. PhD Thesis, Ecole Nationale des Ponts et Chaussées, Université
321 Paris-Est, 2011.

322 [2] Y.J. Cui, T.V. Duong, A.M. Tang, J.C. Dupla, N. Calon, A. Robinet, Investigation of the
323 hydro-mechanical behaviour of fouled ballast, Journal of Zhejiang University Science A.
324 14(4) (2013) 244-255.

325 [3] V.N. Trinh, A.M. Tang, Y.J. Cui, J.C. Dupla, J. Canou, N. Calon, L. Lambert, A. Robinet,
326 O. Schoen, Mechanical characterisation of the fouled ballast in ancient railway track
327 substructure by large-scale triaxial tests, Soils and foundations. 52(3) (2012) 511-523.

328 [4] T.V. Duong, A.M. Tang, Y.J. Cui, V.N. Trinh, J.C. Dupla, N. Calon, J. Canou, A. Robinet,
329 Effects of fines and water contents on the mechanical behavior of interlayer soil in
330 ancient railway sub-structure, Soils and foundations. 53(6) (2013) 868-878.

331 [5] T.V. Duong, Y.J. Cui, A.M. Tang, J.C. Dupla, J. Canou, N. Calon, A. Robinet,
332 Investigating the mud pumping and interlayer creation phenomena in railway sub-
333 structure, Engineering geology. 171 2014 45-58.

334 [6] T.V. Duong, Y.J. Cui, A.M. Tang, J.C. Dupla, J. Canou, N. Calon, A. Robinet, Effects of
335 water and fines contents on the resilient modulus of the interlayer soil of railway
336 substructure, Acta Geotechnica. 11(1) 2016 51-59.

337 [7] F. Lamas-Lopez, S.C. d'Aguiar, A. Robinet, Y.J. Cui, N. Calon, J. Canou, J.C. Dupla,
338 A.M. Tang, In-situ investigation of the behaviour of a French conventional railway

platform, In Proceedings of the transportation research board 94th annual meeting. Washington, DC (2015) 15-1076.

[8] F. Lamas-lopez, Field and laboratory investigation on the dynamic behavior of conventional railway track-bed materials in the context of traffic upgrade. PhD Thesis, Ecole Nationale des Ponts et Chaussées, Université Paris-Est, 2016.

[9] H.L. Wang, Y.J. Cui, F. Lamas-Lopez, J.C. Dupla, J. Canou, N. Calon, G. Saussine, P. Aimedieu, R.P. Chen, Effects of inclusion contents on resilient modulus and damping ratio of unsaturated track-bed materials, Canadian Geotechnical Journal. 54(12) (2017) 1672-1681.

[10] H.L. Wang, Y.J. Cui, F. Lamas-Lopez, N. Calon, G. Saussine, J.C. Dupla, J. Canou, P. Aimedieu, R.P. Chen, Investigation on the mechanical behavior of track-bed materials at various contents of coarse grains, Construction and Building Materials. 164 (2018) 228-237.

[11] H.L. Wang, Y.J. Cui, F. Lamas-Lopez, J.C. Dupla, J. Canou, N. Calon, G. Saussine, P. Aimedieu, R.P. Chen, Permanent deformation of track-bed materials at various inclusion contents under large number of loading cycles, Journal of Geotechnical and Geoenvironmental Engineering. 144(8) (2018) 04018044.

[12] S. Qi, Y.J. Cui, R.P. Chen, H.L. Wang, F. Lamas-Lopez, P. Aimedieu, J.C. Dupla, J. Canou, G. Saussine, Influence of grain size distribution of inclusions on the mechanical behaviours of track-bed materials, Géotechnique. (2019) 1-10.

359 [13] B. Seif El Dine, J. C. Dupla, R. Frank, J. Canou, Y. Kazan, Mechanical characterization
360 of matrix coarse-grained soils with a large-sized triaxial device, Canadian Geotechnical
361 Journal. 47(4) (2010) 425-438.
362 [14] L.E. Vallejo, Interpretation of the limits in shear strength in binary granular mixtures,
363 Canadian Geotechnical Journal. 38(5) (2001) 1097-1104.
364 [15] ASTM D698-12. Standard test methods for laboratory compaction characteristics of soil
365 using standard effort. ASTM International, West Conshohocken, Pa, 2012)
366 [16] P.A. Vermeer, R. De Borst, Non-associated plasticity for soils, concrete and rock.
367 HERON, 29(3) (1984) 1-64.
368 [17] Y.J. Cui, P. Delage, Yeilding and plastic behaviour of an unsaturated compacted silt,
369 Géotechnique. 46(2) (1996) 291-311.
370 [18] C.W.W. Ng, S. Baghbanrezvan, H. Sadeghi, C. Zhou, F. Jafarzadeh, Effect of specimen
371 preparation techniques on dynamic properties of unsaturated fine-grained soil at high
372 suctions, Canadian Geotechnical Journal. 54(9) (2017) 1310-1319.
373 [19] H.F. Zhao, L.M. Zhang, D.G. Fredlund, Bimodal shear-strength behavior of unsaturated
374 coarse-grained soils, Journal of geotechnical and geoenvironmental engineering. 139(12)
375 (2013) 2070-2081.
376 [20] R. de Frias Lopez, J. Silfwerbrand, D. Jelagin, B. Birgisson, Force transmission and soil
377 fabric of binary granular mixtures, Géotechnique. 66(7) (2016)578-583.
378 [21] L.M. Zhang, X. Li, Microporosity structure of coarse granular soils, Journal of
379 Geotechnical and Geoenvironmental Engineering. 136(10) (2010)1425-1436.

380 [22] J.C. Fiès, N.D.E., Louvigny, A. Chanzy The role of stones in soil water retention,
381 European Journal of Soil Science. 53(1) (2002) 95-104.

382 NOTATIONS

c	cohesion
E_0	initial Young's modulus
f_v	volumetric coarse grain content
$f_{v\text{-}cha}$	characteristic volumetric coarse grain content
k_c	slope of volume change curve in the contractancy phase
k_D	slope of volume change curve in the dilatancy phase
ρ_d	dry density of sample
$\rho_{dmax\text{-}f}$	maximum dry density of fine soil
q	deviator stress
q_{max}	peak deviator stress
$w_{opt\text{-}f}$	optimum water content of fine soil
w_f	water content of fine soil
ε_a	axial strain
ε_v	volumetric strain
σ_3	confining pressure
φ	friction angle
v	Poisson's ratio
ψ	dilatancy angle

383

384

385 LIST OF TABLES

Table 1. The constitution of fine soil
Table 2. Experimental program
Table 3. Suction and water content measured at different equilibration times for fine soils
Table 4. $f_{v\text{-}cha}$ values at different water contents

386

387 LIST OF FIGURES

Fig. 1. Grain size distribution curves of fine soils (after Wang et al. [10])
Fig. 2. Plasticity of fine soils (after Wang et al. [10])
Fig. 3. Samples states with respect to the compaction curve
Fig. 4. Grain size distribution curves of micro-ballast and ballast (after Wang et al. [10])
Fig. 5. Volume change of samples at different f_v values for the three target water contents
Fig. 6. Results from the tests at w_1=17.6% and different f_v values under: (a_1) - (b_1) σ_3= 30 kPa; (a_2) - (b_2) σ_3= 60 kPa; (a_3) - (b_3) σ_3= 120 kPa
Fig. 7. Variations of peak deviator stress with f_v under different σ_3 values for: (a) w_1 = 17.6%; (b) w_2 = 10.6%; (c) w_3 = 7.0%
Fig. 8. Variations of initial Young's modulus with f_v under different σ_3 values for: (a) w_1 = 17.6%; (b) w_2 = 10.6%; (c) w_3 = 7.0%
Fig. 9. Variations of Poisson's ratio with f_v under different σ_3 values for: (a) w_1 = 17.6%; (b) w_2 = 10.6%; (c) w_3 = 7.0%
Fig. 10. Variations of dilatancy angle with f_v under different σ_3 values for: (a) w_1 = 17.6%; (b) w_2 = 10.6%; (c) w_3 = 7.0%
Fig. 11. Variations of cohesion with f_v under different water contents
Fig. 12. Variations of friction angle with f_v under different water contents

388

389 Table 1. The constitution of fine soil

Soil	Mass proportion (%)	Grain size range (mm)
HN34	3.3	0.063 - 0.50
HN31	3.3	0.16 - 0.63
HN0.4-0.8	6.7	0.25 - 1
HN0.6-1.6	6.7	0.32 - 2
HN1-2.5	13.3	0.32 – 3.20
C4	16.7	0.0009 – 0.50
C10	20	0.0009 – 0.25
Speswhite	23.3	0.0003 – 0.01
Bentonite	6.7	0.001 – 0.01

390

391

392 Table 2. Experimental program

f_v (%)	Initial water content w_{opt-f} (%)	Target w_f (%)	Target S_r (%)	Target ρ_{dmax-f} (Mg/m^3)	Target ρ_d (Mg/m^3)	Measured ρ_d (Mg/m^3)	Confining pressure σ_3 (kPa)		
		17.6	100			1.80	30	60	120
0		10.6	60		1.82	1.85	30	60	120
		7.0	40			1.86	30	60	120
		17.6	100			1.88	30	60	120
10		10.6	60		1.91	1.93	30	60	120
		7.0	40			1.94	30	60	120
		17.6	100			1.97	30	60	120
20	13.7	10.6	60	1.82	1.99	2.01	30	60	120
		7.0	40			2.03	30	60	120
		17.6	100			2.11	30	60	120
35		10.6	60		2.12	2.13	30	60	120
		7.0	40			2.13	30	60	120
		17.6	100			2.20	30	60	120
45		10.6	60		2.21	2.22	30	60	120
		7.0	40			2.23	30	60	120

Note: f_v represents the ratio of volumetric inclusion content to the total volume of the sample [10]. w_{opt-f}, w_f, S_r and ρ_{dmax-f} represent the optimum water content, the water content, the degree of saturation and the maximum dry density of fine soils, respectively. ρ_d represents the dry density of soil mixture sample. Measured ρ_d represents the dry density of soil mixture sample after wetting or drying from compaction water content w_{opt-f} to target w_f.

Table 3. Suction and water content measured at different equilibration times for fine soils

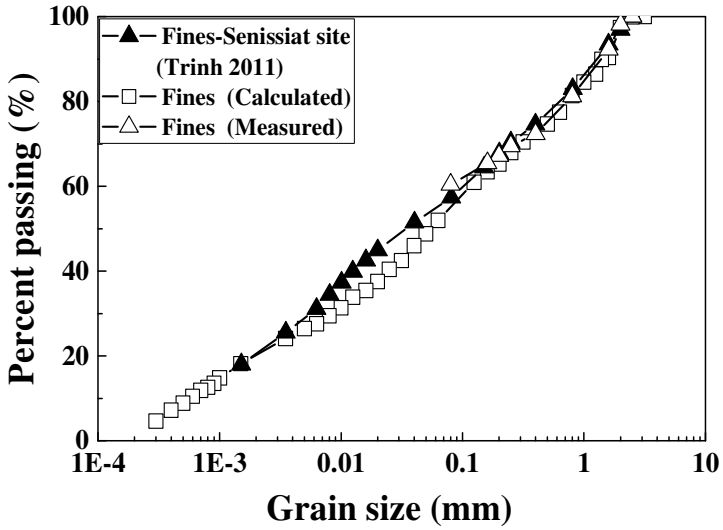
Position	Suction (MPa)	Water content (%)	Suction (MPa)	Water content (%)
	After 6h		After 7h	
center	0.33	12.7	0.32	12.9
1/2 r	0.24	13.5	0.35	12.8
r	0.46	13.7	0.33	13.1

Table 4. $f_{v\text{-}cha}$ values at different water contents

w (%)	17.6	13.7	10.6	7.0
$f_{v\text{-}cha}$ (%)	25	27	29	33

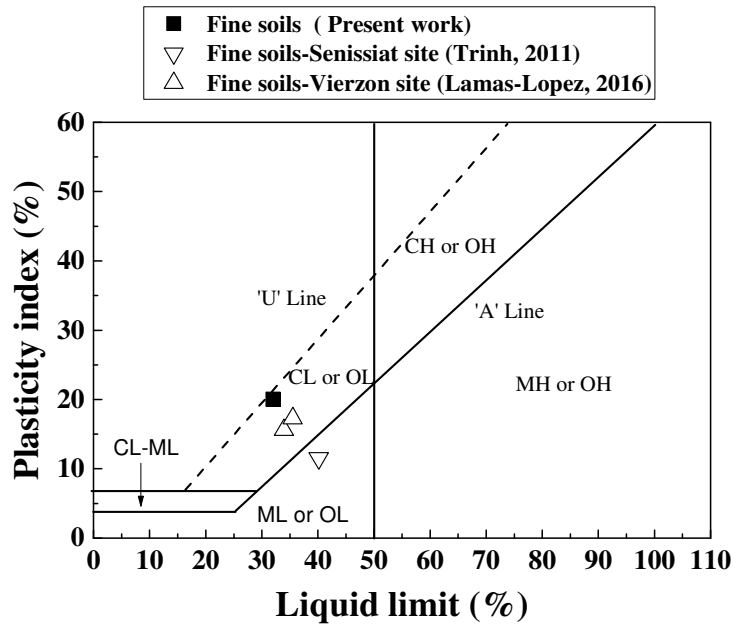
Note: $f_{v\text{-}cha} \approx 27\%$ corresponding to $w = 13.7\%$ was obtained by Wang et al. [10]

393



394

Fig. 1. Grain size distribution curves of fine soils (after Wang et al. [10])



395

Fig. 2. Plasticity of fine soils (after Wang et al. [10])

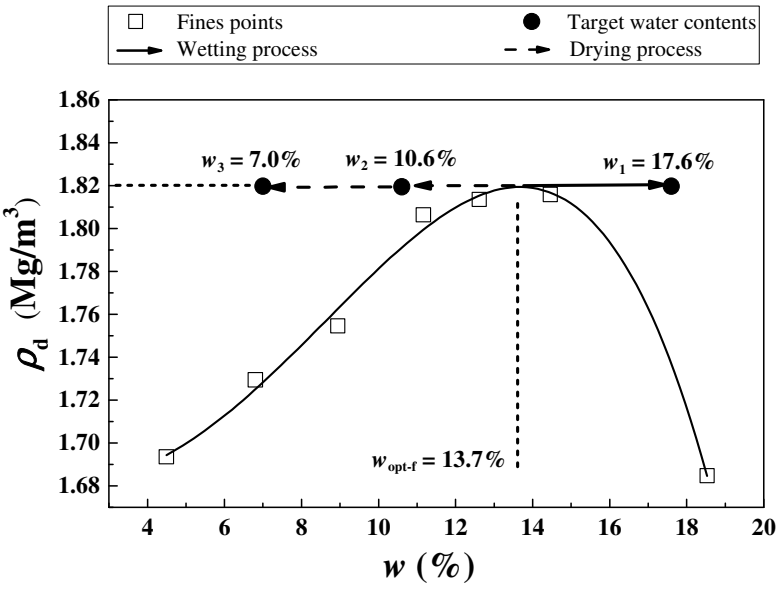
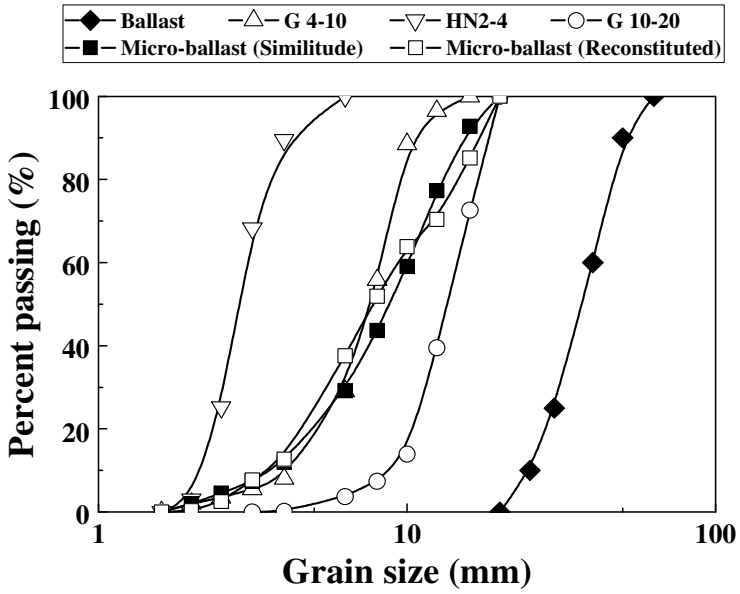


Fig. 3. Samples states with respect to the compaction curve



396

Fig. 4. Grain size distribution curves of micro-ballast and ballast (after Wang et al. [10])

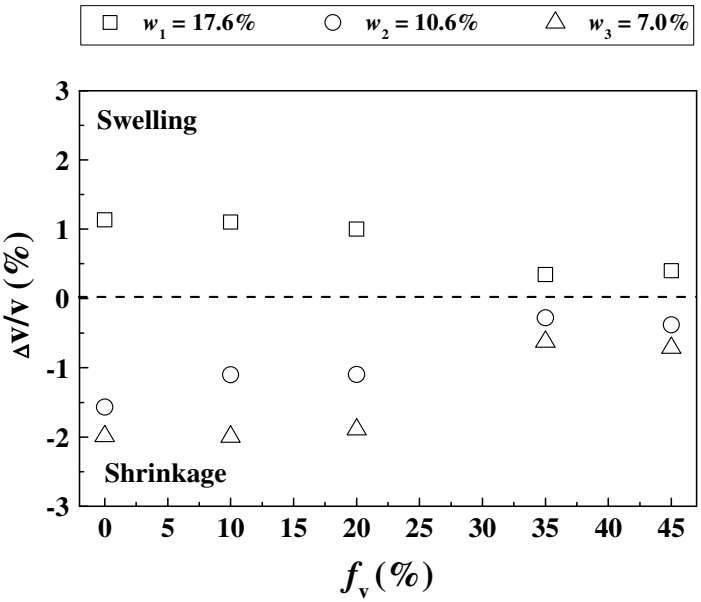
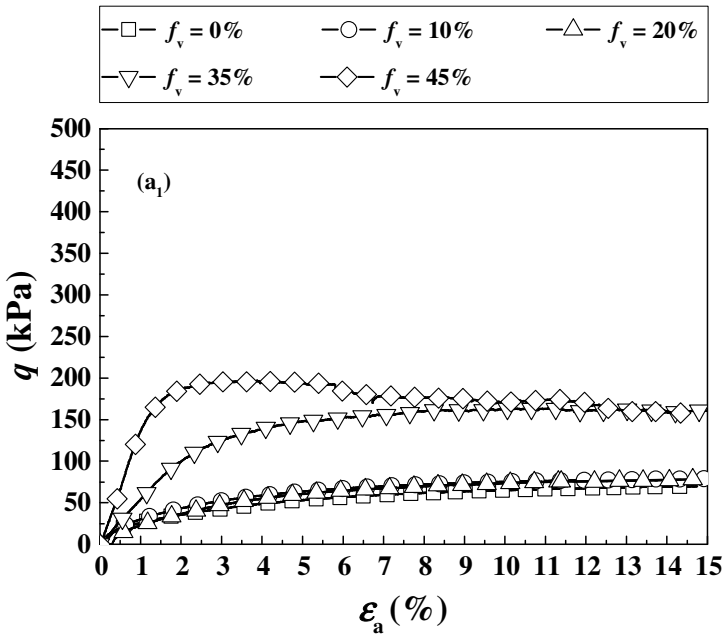
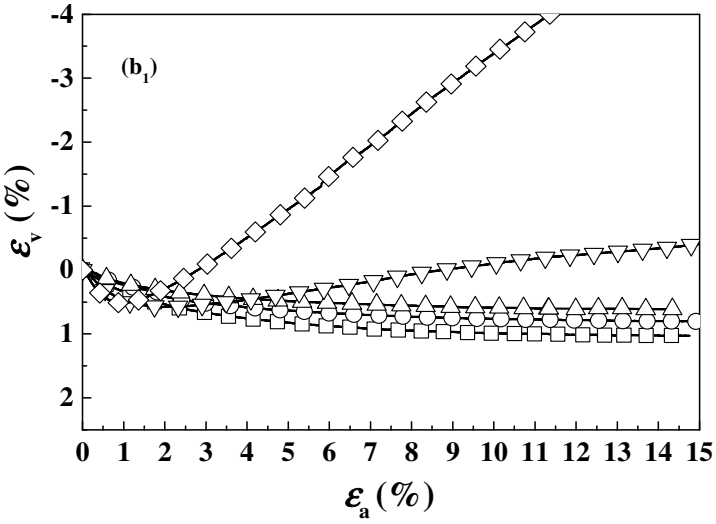


Fig. 5. Volume change of samples at different f_v values for the three target water contents



404



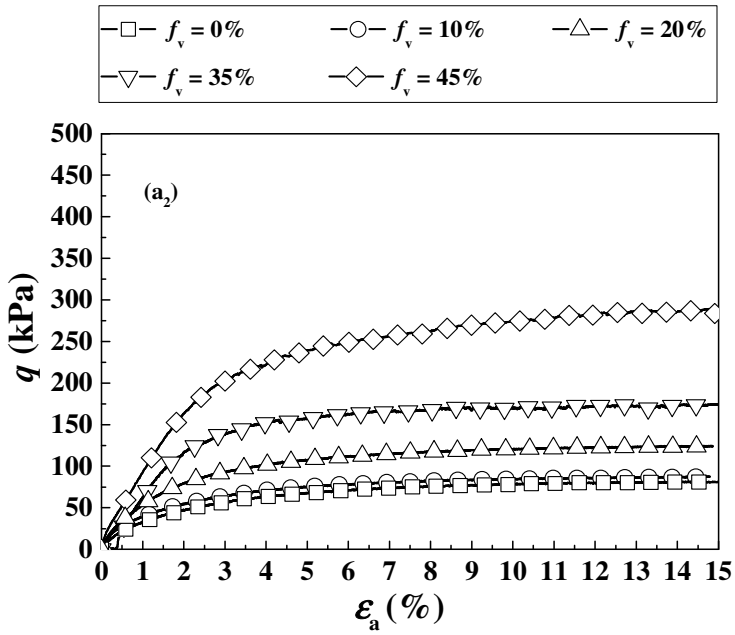
405

406

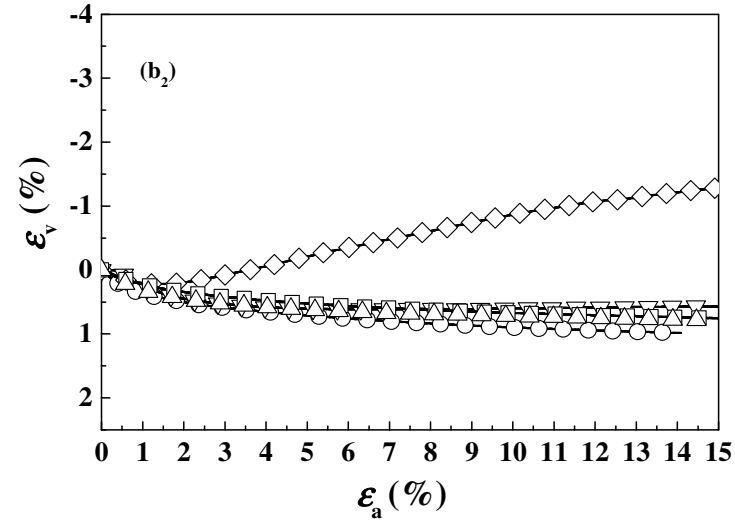
407

408

409



410



411

412

413

414

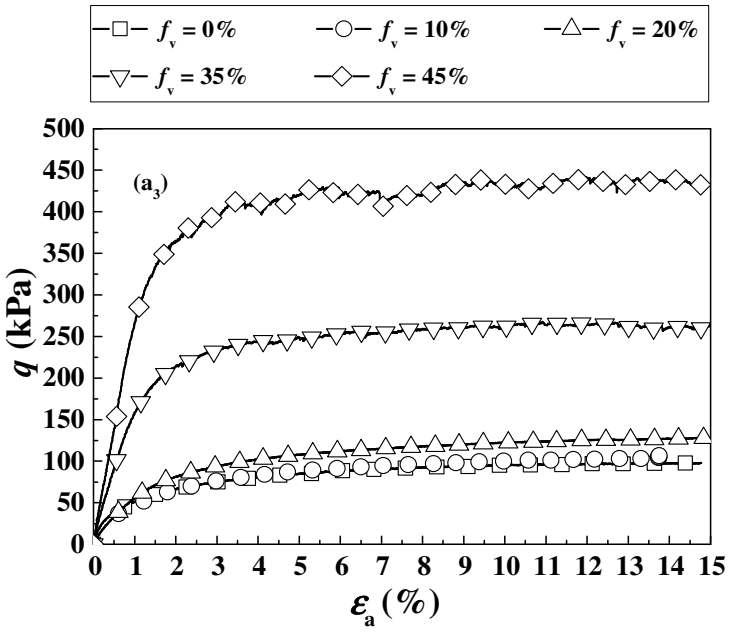
415

416

417

418

419



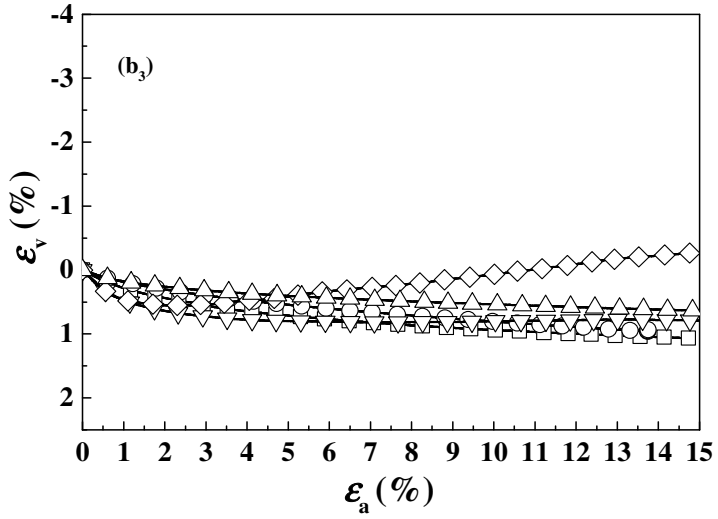
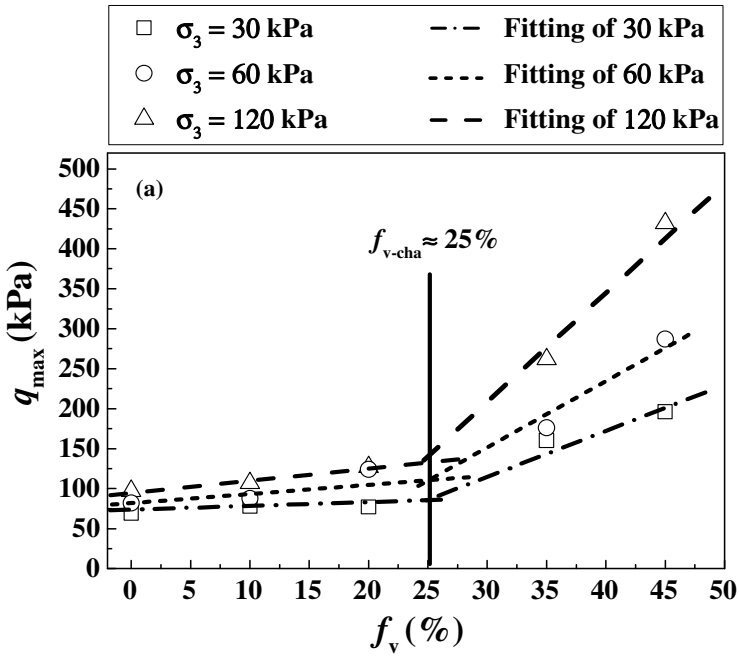
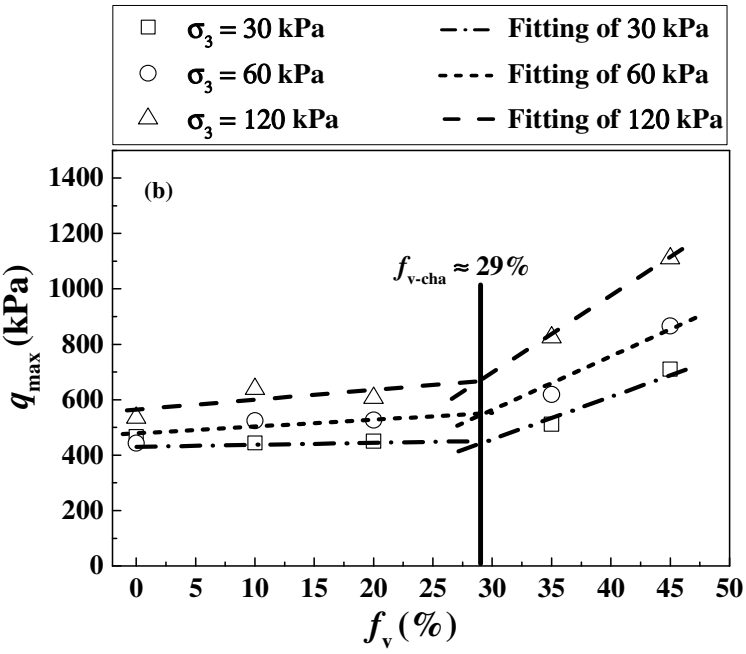
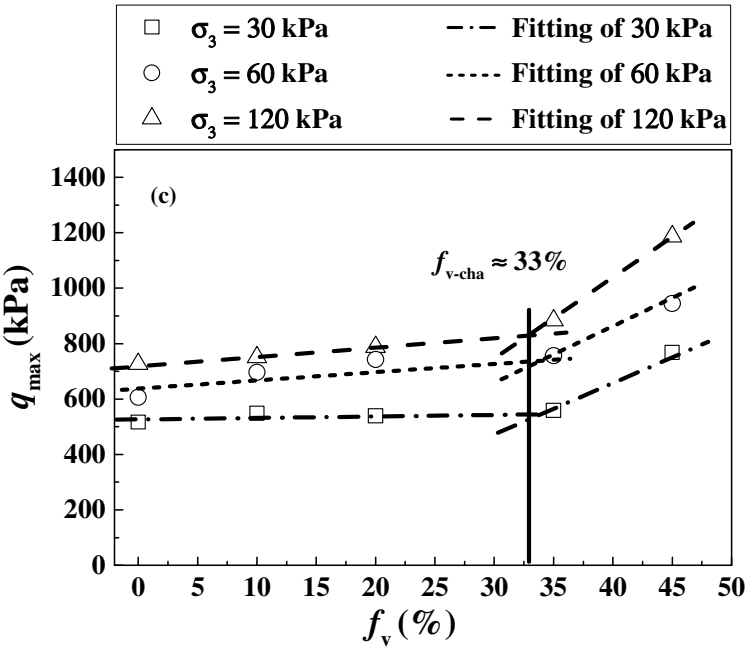


Fig. 6. Results from the tests at w_1=17.6% and different f_v values under:

(a_1) - (b_1) σ_3= 30 kPa; (a_2) - (b_2) σ_3= 60 kPa; (a_3) - (b_3) σ_3= 120 kPa


□ σ3 = 30 kPa
○ σ3 = 60 kPa
△ σ3 = 120 kPa
Fitting of 30 kPa
Fitting of 60 kPa
Fitting of 120 kPa
(a)
fv-cha ≈ 25%
qmax (kPa)
fv (%)
0
50
100
150
200
250
300
350
400
450
500
0
5
10
15
20
25
30
35
40
45
50


□ σ3 = 30 kPa
○ σ3 = 60 kPa
△ σ3 = 120 kPa
Fitting of 30 kPa
Fitting of 60 kPa
Fitting of 120 kPa
(b)
fv-cha ≈ 29%
qmax (kPa)
fv (%)
0
200
400
600
800
1000
1200
1400
0
5
10
15
20
25
30
35
40
45
50



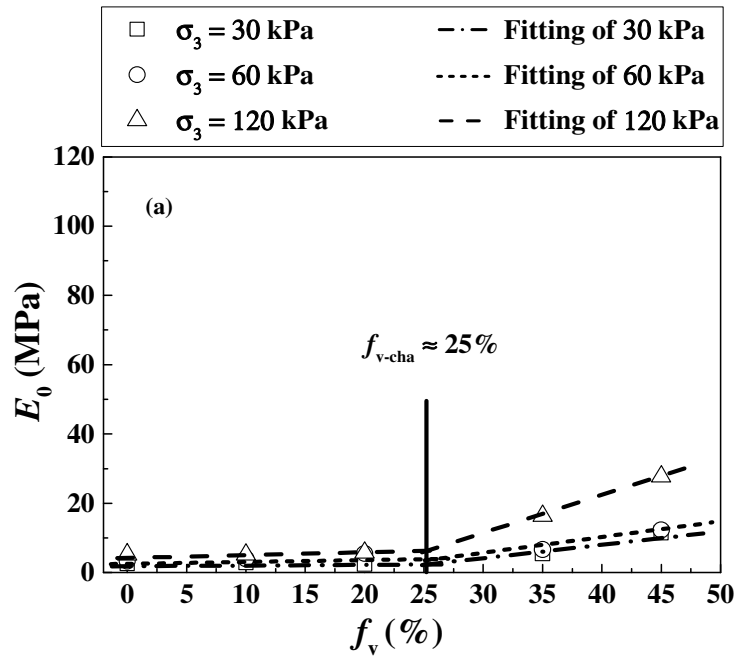
437

438 Fig. 7. Variations of peak deviator stress with f_v under different σ_3 values for:

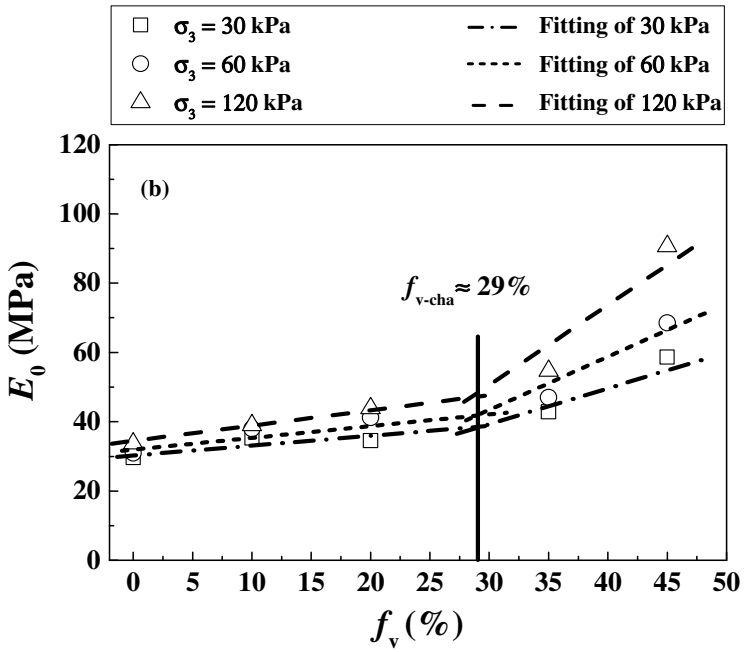
439 (a) $w_1 = 17.6\%$; (b) $w_2 = 10.6\%$; (c) $w_3 = 7.0\%$

440

441



442



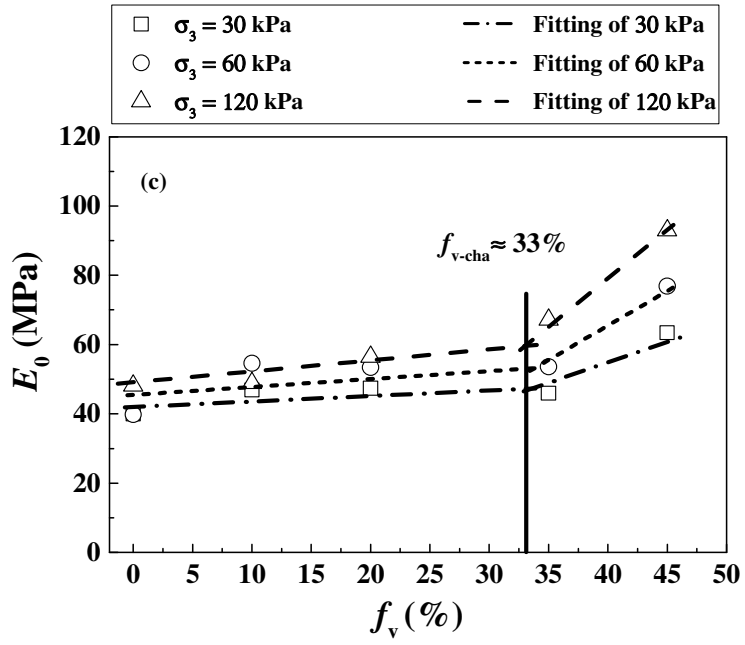
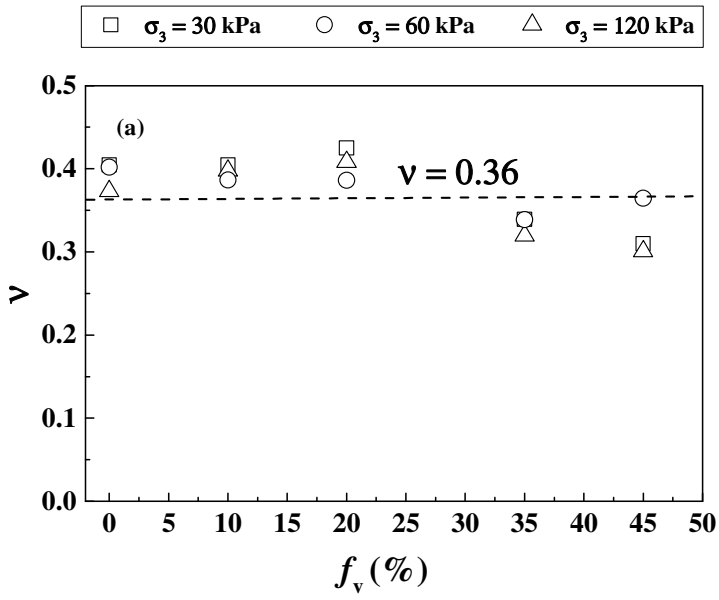
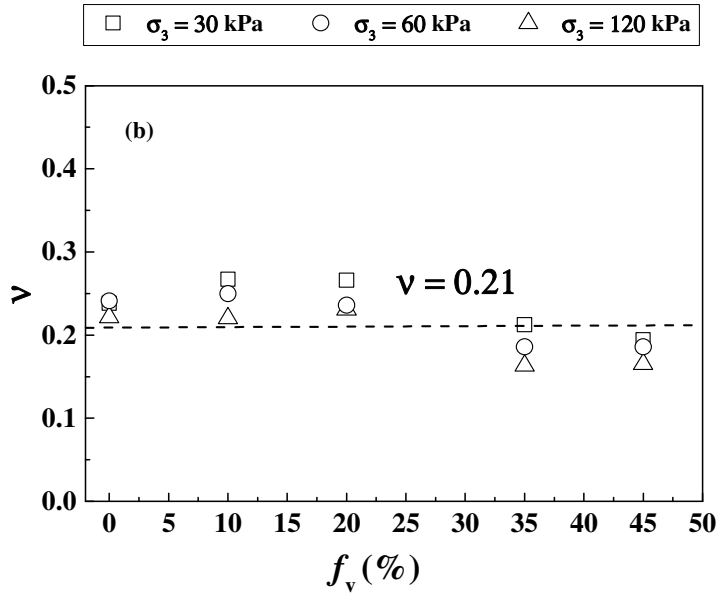


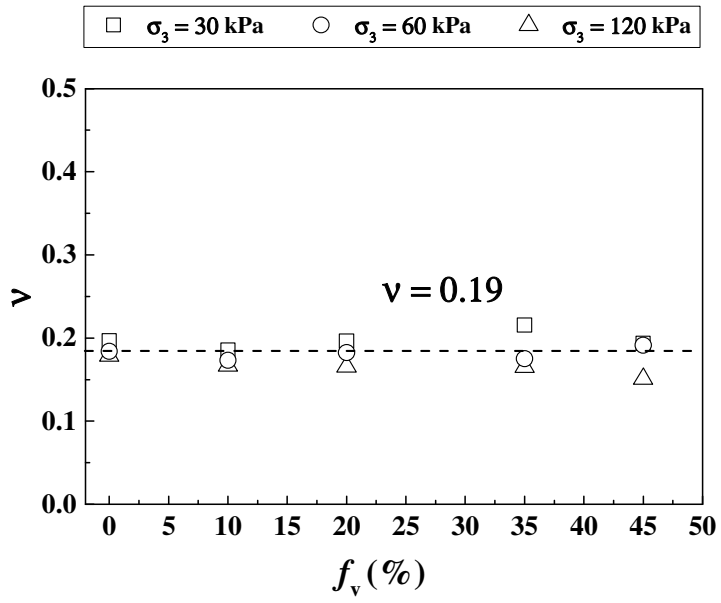
Fig. 8. Variations of initial Young's modulus with f_v under different σ_3 values for: (a) $w_1 = 17.6\%$; (b) $w_2 = 10.6\%$; (c) $w_3 = 7.0\%$


□ σ3 = 30 kPa
○ σ3 = 60 kPa
△ σ3 = 120 kPa
(a)
ν = 0.36
ν
0.0
0.1
0.2
0.3
0.4
0.5
0 5 10 15 20 25 30 35 40 45 50
fv (%)

453


□ σ3 = 30 kPa
○ σ3 = 60 kPa
△ σ3 = 120 kPa
(b)
ν = 0.21
ν
0.0
0.1
0.2
0.3
0.4
0.5
0 5 10 15 20 25 30 35 40 45 50
fv (%)

454

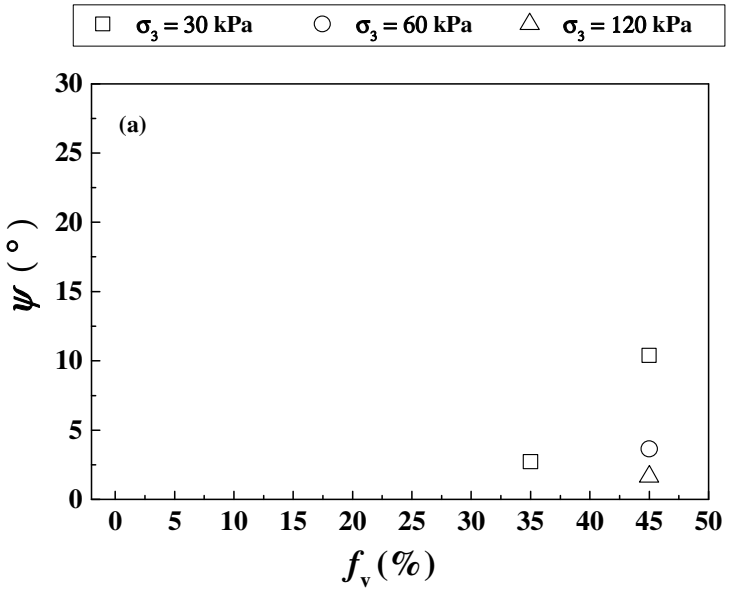


455

456 Fig. 9. Variations of Poisson's ratio with f_v under different σ_3 values for:

457 (a) $w_1 = 17.6\%$; (b) $w_2 = 10.6\%$; (c) $w_3 = 7.0\%$

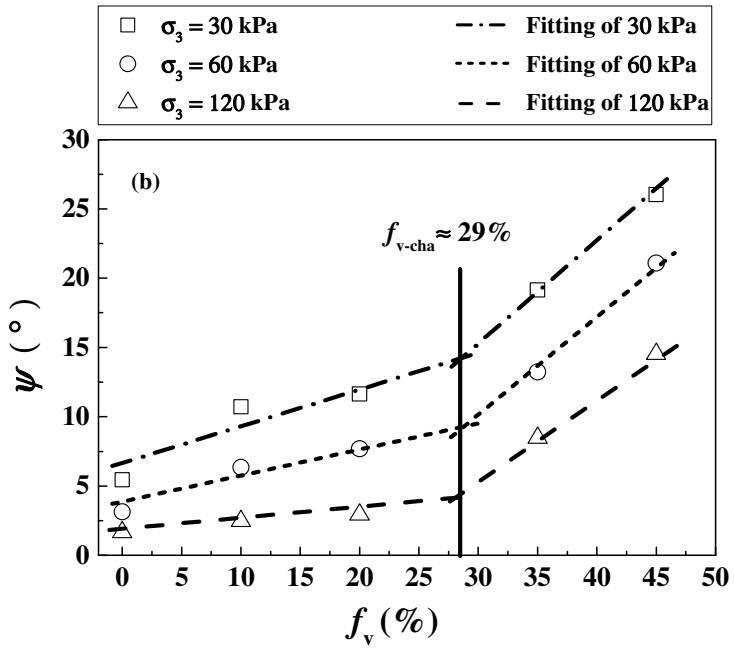
458



459

460

461



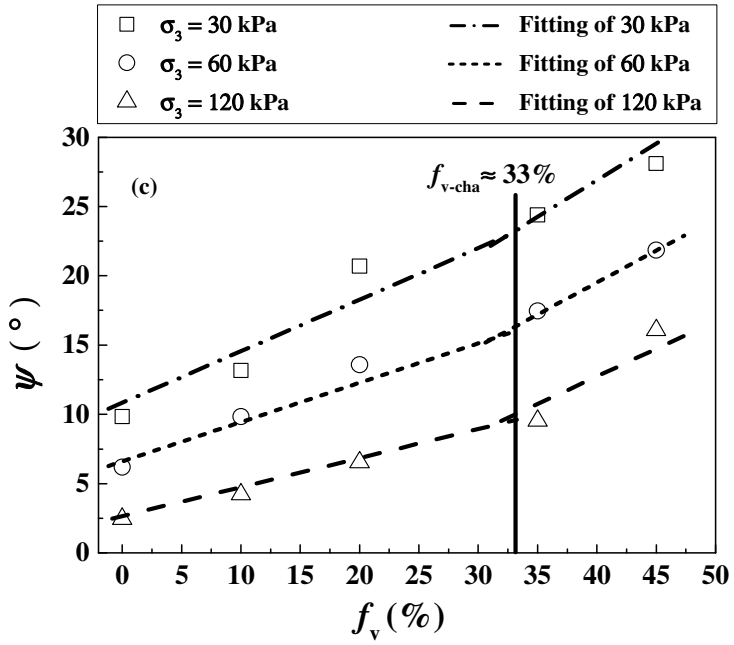


Fig. 10. Variations of dilatancy angle with f_v under different σ_3 values for: (a) $w_1 = 17.6\%$; (b) $w_2 = 10.6\%$; (c) $w_3 = 7.0\%$

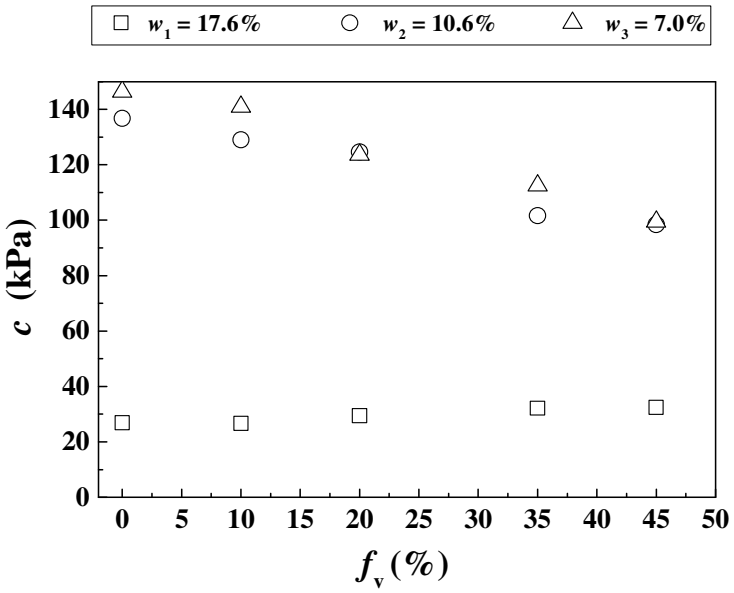


Fig. 11. Variations of cohesion with f_v under different water contents

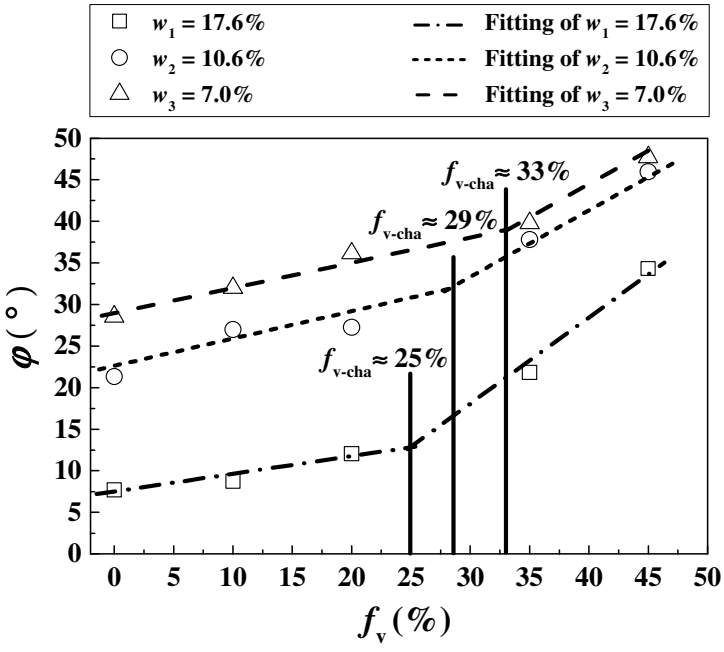


Fig. 12. Variations of friction angle with f_v under different water contents